Accurate Solution of Exterior Helmholtz Problems in Curved 3D Domains Using Geometry-Based p-Version Finite Elements *

Saikat Dey
Naval Research Laboratory/SFA Inc.
1401 McCormick Drive, Largo, MD 20774-5322.
Voice: (202) 767-7321
FAX: (202) 404-7420
email:dey@cosmic.nrl.navy.mil

November 6, 1997

Abstract

This paper describes a method that combines the superior approximation properties of p-version finite element methods with exactly mapped element geometries for highly accurate numerical solution of acoustic radiation problems in three-dimensions for complex geometric domains. Examples show the ability of this method to yield exponentially convergent finite element solutions with less than 1% error in normalized L_2 and H_1-semi norms with very coarse meshes. The method is also unique because it allows finite element analysis based on exact domain geometry as defined in a CAD system which enables easy integration of the analysis process into the design cycle.

Keywords: acoustics, Helmholtz's equation, p-finite elements, exact geometric mapping.

*Research described in this paper was done while the author was a *Postdoctoral Research Associate* at Scientific Computation Research Center, Rensselaer Polytechnic Institute, Troy NY 12180.

1 Introduction

Problems in acoustics involve the solution of the Helmholtz equation given by

$$\Delta\phi + k^2\phi = -f \tag{1}$$

with appropriate boundary conditions in exterior infinite domains [8], where ϕ is the acoustic pressure, k is the wavenumber defined by $k = \frac{\omega}{c}$, ω and c being the frequency and speed of the wave, respectively, and f defines the acoustic source. Finite element methods have emerged as the leading numerical techniques for the solution of problems in structural acoustics [5] and other engineering problems that are governed by partial differential equations over arbitrary geometric domains [9, 19, 16]. Two issues that must be dealt with in the application of finite element method to accurately solve equation (1) are:

1. Control of dispersion error for large wave numbers, and
2. Control of geometric approximation error with high order discretizations.

Understanding and control of dispersion error with Galerkin finite elements is an area of active research [1, 4, 10]. Recently, stabilized finite elements, developed for the solution of advection-diffusion type problems, have been successfully applied for controlling dispersion error [17] in acoustics problems. Use of low order h-version finite elements, in general, offer only algebraic rates of error convergence, and when un-stabilized lead to excessive pollution of the finite element solution due to dispersion if the mesh is not sufficiently refined. Reference [8] states that as a rule-of-thumb 10 linear elements per wavelength are necessary to obtain numerical solutions with acceptable errors. Investigations with quadratic elements show that the quantity k^3h^2, where h defines the measure of element size, must be controlled [4]. In three dimensions, these requirements on the mesh size lead to a large number of elements which increases the cost of achieving a given level of error. In contrast, p-version finite element discretization, for properly designed meshes, can yield exponential rates of error convergence [3, 11] and, in addition, allow the use of much coarser meshes without incurring excessive dispersion error.

To highlight the reduction in the mesh size with high p elements, the following constraints on mesh size based on *a-priori* dispersion error analysis given in [10] are used:

C1 (Asymptotic)

$$\frac{hk^2}{p} < \frac{1}{\sqrt{12}} \tag{2}$$

C2 (Pre-Asymptotic)

$$k(\frac{hk}{2p})^p \leq \check{c} \tag{3}$$

$\check{c}$ is a small number; compatibility of **C1** and **C2** when $p = 1$ requires $\check{c} = \frac{1}{4\sqrt{3}}$. To estimate the effect of these constraints on the mesh sizes in three-dimensions, consider a domain that is an octant of a unit sphere. If N_r is the number of elements in the radial direction per unit length, then the total number of elements grows asymptotically as $N_e = 8^{\log_2 N_r}$. Approximating $h \approx \frac{1}{N_r}$ would lead to

$$N_r > \begin{cases} \frac{\sqrt{12}k^2}{p} \text{ if C1} \\ \\ \frac{k}{2p(\frac{\check{c}}{k})^{\frac{1}{p}}} \text{ if C2} \end{cases} \tag{4}$$

Figure 1 plots the growth of N_r as k increases for $p = 1, 2$. Clearly, the growth rate of N_r (and hence total elements) is much smaller with increasing p. Constraint **C1** is designed to drive the local dispersion error to zero. For practical problems the use of the weaker constraint **C2** suffices [10]. Table 1 lists number of elements predicted using **C2** for varying k and p. Although these numbers are rough estimates based on specific assumptions, the importance of using high p is obvious from the reduction in the number of elements.

The use of coarse meshes with p-elements implies that individual finite elements cover large portions of the curved problem domain. This requires that the curvilinear geometry of the finite elements be represented accurately enough so that the errors in finite element geometry approximation do not reduce the rate of convergence of the total finite element error. Reference

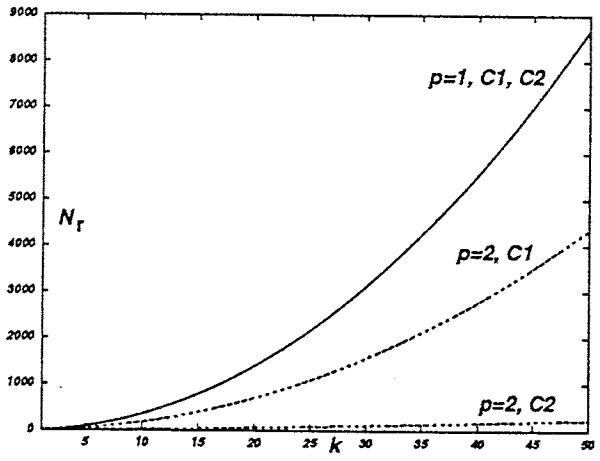

Figure 1: Growth of N_r.

	k=1	k=5	k=10	k=20
p=1	64	262144	16777216	1073741824
p=2	1	512	4096	262144
p=3	1	64	512	4096
p=4	1	8	64	512

Table 1: Asymptotic number of elements based on **C2**.

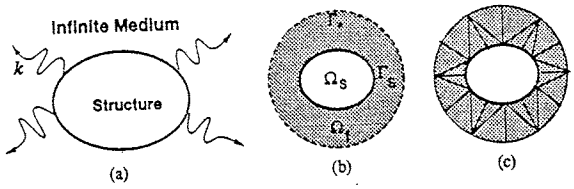

Figure 2: Model problem: (a) physical description, (b) computational domain, and (c) finite element model.

[7] describes a technique based on blending functions to construct geometric mappings for finite elements that conform exactly to the mathematical description of the domain geometry housed within a CAD system. Since this technique eliminates all geometric approximation errors, it is well suited for use with higher-order finite element methods.

This paper presents a technique that combines the p-version Galerkin finite element method with exact geometric mapping to yield accurate numerical solutions for exterior Helmholtz problems. The rest of the paper is organized as follows: Section 2 describes the model problem and its finite element discretization. Section 3 describes the mesh-topology-based variable-order hierarchic shape functions used in the discretization. Section 4 defines the construction of the exact mesh geometric mapping. Numerical examples are presented in Section 5. Conclusions are presented in Section 6.

2 Model Problem and Finite Element Discretization

2.1 Physical and Mathematical Description

The physical description of the model problem considered in this paper is acoustic radiation with wavenumber k from a rigid structure submerged in an infinite acoustic medium as shown Figure 2(a). The problem domain is made finite by truncating the infinite exterior with an artificial boundary denoted by Γ_*. The resulting computational model is represented in Figure 2(b).

In the absence of any source in the fluid domain ($f = 0$), the strong form of the governing partial differential equation is given by

$$\Delta\phi + k^2\phi = 0, \ in \ \Omega_f \tag{5}$$

$$\frac{\partial\phi}{\partial n} = h, \ on \ \Gamma_s \tag{6}$$

$$\frac{\partial\phi}{\partial n} = I\phi, \ on \ \Gamma_* \tag{7}$$

where n defines the unit normal pointing into Ω_f. The operator I defines the appropriate non-reflecting radiation boundary condition at infinity. The choice of accurate boundary conditions on Γ_* is very important and a number of solutions have been proposed. Reference [15] has a comprehensive bibliography on this subject. However, since it is not the focus of this paper, I , for the present discussion, will be based either on approximating the *Sommerfeld* radiation condition

$$\lim_{r\to\infty} \frac{\partial\phi}{\partial r} = ikp$$

by using $I = ik$, or by applying the exact boundary condition at infinity - which is available for the special case when Γ_* is spherical.

Application of standard Galerkin techniques to equation (5) leads to the following variational or *weak* statement the problem:

Given h, I, trial function space $U \subset H^1(\Omega_f)$, and weighting function space $W \subset H^1(\Omega_f)$, find $\phi \in U : \overline{\Omega_f} \to C$ such that $\forall\ w \in W : \overline{\Omega_f} \to C$

$$a(w,\phi) \ - \ k^2(w,\phi) \ - \ (w, I\phi)_{\Gamma_*} \ = \ (w,h)_{\Gamma_s} \tag{8}$$

with

$$a(w,\phi) \ = \ \int_{\Omega_f} \nabla w \cdot \nabla\phi \, d\Omega, \tag{9}$$

$$(w,\phi) \ = \ \int_{\Omega_f} w\phi \, d\Omega, \tag{10}$$

$$(w, I\phi)_{\Gamma_*} \ = \int_{\Gamma_*} wI\phi \, d\Gamma, \tag{11}$$

$$(w,h)_{\Gamma_s} \ = \int_{\Gamma_s} wh \, d\Gamma \tag{12}$$

2.2 Finite Element Discretization

The computational domain is discretized by conforming finite elements as shown in Figure 2(c) and following the standard technique [9] the trial and weighting functions are approximated as piecewise polynomials of degree p defined over individual finite elements of size h

$$w^{(h,p)} = \sum_{i=1}^{n_p} N_i w_i^{(h,p)} \tag{13}$$

$$\phi^{(h,p)} = \sum_{i=1}^{n_p} N_i \phi_i^{(h,p)} \tag{14}$$

where n_p is the total number of shape functions which is based on the topology of the element. For tetrahedra (used here) $N_p = (p+1)(p+2)(p+3)/6$; expressions for other topologies are given in [6].

Substitution of the discretized trial and weighting functions into equation (8) leads to the matrix form of the problem given by

$$[K - k^2 M - D]\phi^{(h,p)} = \mathbf{r} \tag{15}$$

where global matrices K, M and D are assembled from the following element level matrices

$$k_{ij} = \int_{\Omega^e} \nabla N_i \cdot \nabla N_j \, d\Omega, \tag{16}$$

$$m_{ij} = \int_{\Omega^e} N_i N_j \, d\Omega, \tag{17}$$

$$d_{ij} = \int_{\Gamma_s^e} N_i I N_j \, d\Gamma, \tag{18}$$

$$r_i = \int_{\Gamma_s^e} N_i h d\Gamma \tag{19}$$

where Ω^e defines the domain of a finite element, $\Gamma_*^e = \partial\Omega^e \cap \Gamma_*$, and $\Gamma_s^e = \partial\Omega^e \cap \Gamma_s$.

Having developed a p-version finite element formulation, the next section describes a general and flexible framework for the specification and evaluation of variable order finite element shape functions over conforming meshes based on [13].

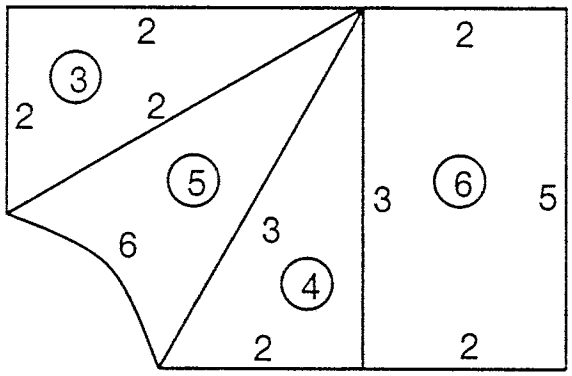

Figure 3: Example of variable p specification.

3 Topology Based Hierarchic Basis Functions

Variable order shape function construction must allow for independent specification of polynomial degrees associated with individual mesh entities (vertices, edges, faces and regions) that belong to the closure of a finite element domain $\overline{\Omega^e}$. In addition, the shape functions are hierarchic in polynomial degree which implies that all shape functions defining an order p basis are a subset of the degree $p+1$ basis [16]. The approximation basis over the domain of an element is defined by the set of all shape functions contributed by entities belonging to the closure of the element. Figure 3 shows an example of variable-p mesh. The number along the edges indicate the degree of approximating polynomial along that edge while those inside the circles indicate the polynomial degrees of the face shape functions. To ensure proper continuity of the finite element solution it is required that the shape functions be C^0 continuous at the inter-element boundaries.

A flexible mesh-topology-based framework for variable-order hierarchic shape functions was developed in reference [13] in which each hierarchic shape function is represented as a product of two functions given by

$$N(p) \;=\; \Psi(\xi)\Phi(p,\xi') \tag{20}$$

where

Φ is a function of the parametric coordinates ξ' of the mesh entity that contributes the shape function and depends on the polynomial degree p attached to that entity,

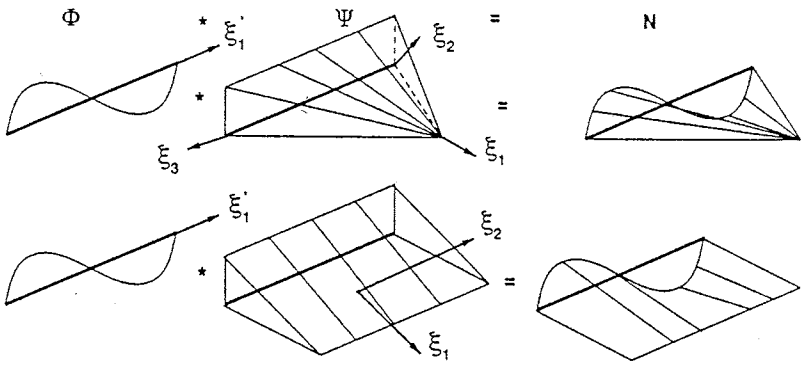

Figure 4: Decomposed edge shape functions.

Ψ is a function associated with the element that blends the entity function Φ over the domain of the element in a manner that makes the resulting product C^0 continuous. It is written in terms of the parametric coordinates of the element, ξ, and is independent of the p associated with mesh entity.

An illustration of this product decomposition is shown in Figure 4. Shape functions constructed in this manner are automatically C^0 continuous, whereas those constructed directly in terms of the element parametric coordinates require a change of sign based on the direction of use of the mesh entity by the specific element [16]. Specific shapes of the edge and face shape functions are shown in Figures 5, 6, 7 and 8. Readers interested in the details of derivation of expressions for Ψ and Φ for various element topologies are referred to [6, 13].

4 Exact Mesh Geometry Mapping

Numerical evaluation of the integrals in (16), for arbitrary curved elements, requires a geometric mapping function $\mathbf{x}(\xi)$ to transform them in terms of

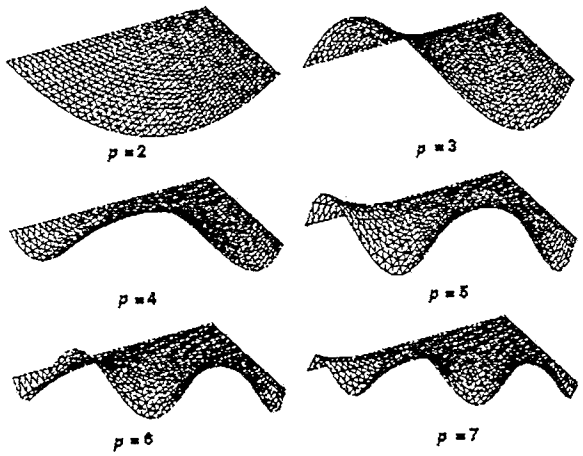

Figure 5: Triangle edge shape functions.

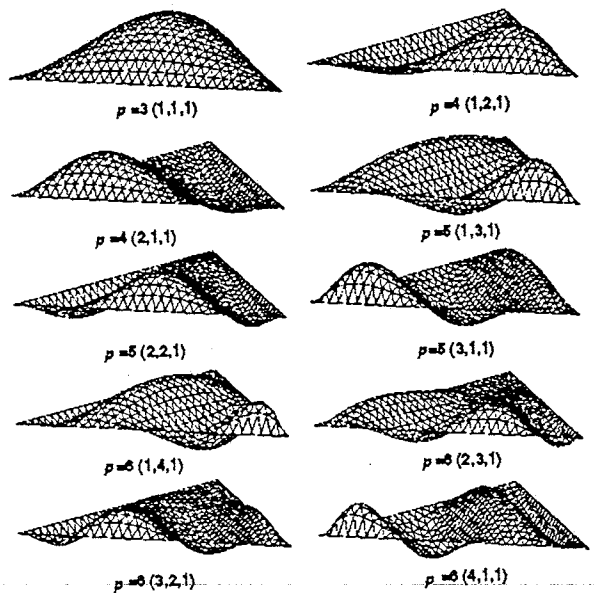

Figure 6: Triangle face shape functions.

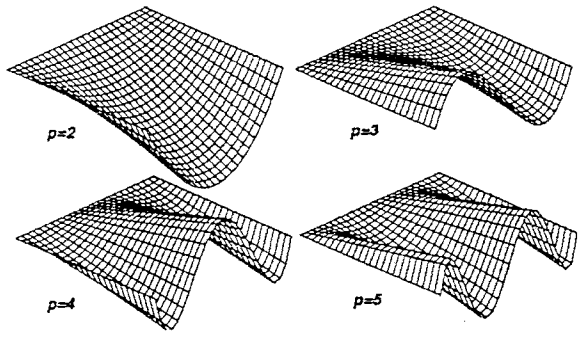

Figure 7: Quadrilateral edge shape functions.

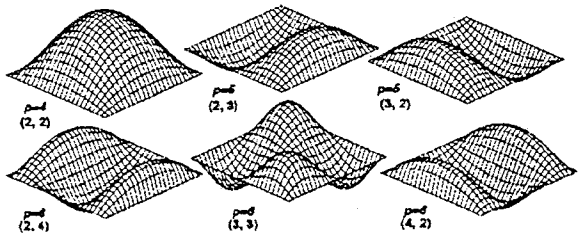

Figure 8: Quadrilateral face shape functions.

the element parametric coordinate system ξ as follows:

$$k_{ij} = \int_{\Omega^e} \frac{\partial N_i}{\partial \xi} \frac{\partial \xi}{\partial \mathrm{x}} \left(\frac{\partial N_j}{\partial \xi} \frac{\partial \xi}{\partial \mathrm{x}}\right)^T J(\xi)\, d\xi, \tag{21}$$

$$m_{ij} = \int_{\Omega^e} N_i(\mathrm{x}(\xi)) N_j(\mathrm{x}(\xi)) J(\xi)\, d\xi, \tag{22}$$

$$d_{ij} = \int_{\Gamma_s^e} N_i(\mathrm{x}(\xi)) I N_j(\mathrm{x}(\xi)) J(\xi)\, d\xi, \tag{23}$$

$$f_i = \int_{\Gamma_s^e} N_i(\mathrm{x}(\xi)) h(\mathrm{x}(\xi)) J(\xi)\, d\xi \tag{24}$$

where $J(\xi) = |\frac{\partial x_i}{\partial \xi_j}|$.

A method to obtain $\mathrm{x}(\xi)$ that is exact with respect to the mathematical definition of the geometry of the problem domain, as defined by a geometric modeling system, was developed in [7]. The procedure is based on mesh *classification* [12, 14] which is the unique association of each mesh entity with a geometric model entity. An abstract representation of the mapping is given by $\mathrm{x}(\xi) = \mathrm{x}(\zeta(\xi))$ is illustrated in Figure 9. The mapping works in two

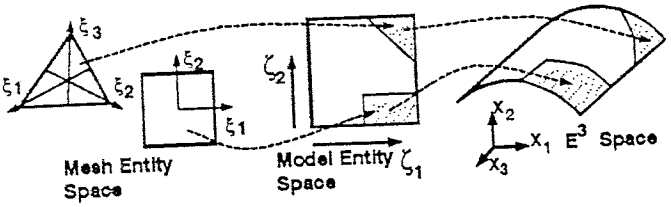

Figure 9: Geometric mapping for mesh face.

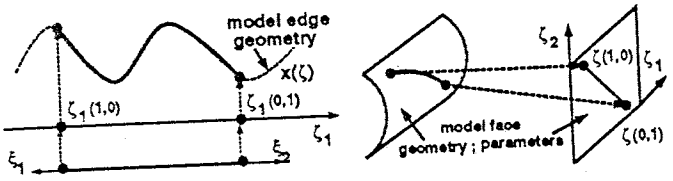

Figure 10: Geometric mapping for mesh edge.

steps: the first step is to construct a mapping $\zeta(\xi)$ to map the finite element parametric coordinates, ξ, to the parametric coordinates of the geometric model entity, ζ, on which the mesh entity is classified; the second step consists of using the mapping $\mathbf{x}(\zeta)$ that is housed within the geometric modeling system. Derivatives of the mapping are obtained by the application of the chain rule $\frac{\partial \mathbf{x}}{\partial \xi} = \frac{\partial \mathbf{x}}{\partial \zeta}\frac{\partial \zeta}{\partial \xi}$. Values of $\mathbf{x}(\zeta)$ and $\frac{\partial \mathbf{x}}{\partial \zeta}$ are queried on a pointwise basis from the geometric modeler. The implicit assumption in this process is that the geometric model entities have an underlying continuous, non-degenerate parametric space. As an example, figure 10 describes the mapping of a mesh edge classified on a geometric model edge (curve) and on a geometric model face (surface). A straightforward choice for $\zeta(\xi)$, in this case, is given by

$$\zeta_i(\xi) = \zeta_i(1,0)\xi_1 + \zeta_i(0,1)\xi_2,\ \xi_1 + \xi_2 = 1. \tag{25}$$

Since most geometric modelers do not have explicit parameterization for solid regions, the mapping for three-dimensional mesh regions is constructed by blending the mapped shapes of the bounding vertices, edges and faces. Details of mesh face and region mappings are available in [7, 6] and will not be repeated here. Instead, Figure 11 presents an example of exact curvilinear mesh for a submarine produced by this mapping procedure.

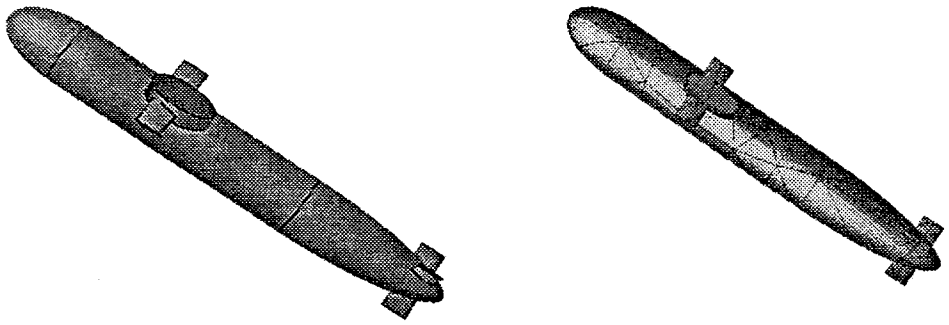

Figure 11: Submarine: geometric model (left) and curvilinear mesh (right).

5 Numerical Examples

The aim of the these numerical examples is to demonstrate that use of p-enrichment along with exact curvilinear mappings can be used to produce very accurate numerical solution, with exponential error convergence, of the Helmholtz equation in complex curved domains in three-dimensions.

All examples consist of solving for the acoustic pressure distribution as a result of acoustic radiation from objects of various shapes for $k = 1$. The shape of Γ_* is prescribed to be a sphere. The boundary condition on Γ_s is specified such that the exact solution is given by

$$\phi(r) = \frac{e^{ikr}}{r} \tag{26}$$

where $r = \sqrt{x^2 + y^2 + z^2}$ defines the radial distance from the center of the sphere defining Γ_*. Exact boundary condition at infinity is enforced by prescribing

$$\frac{\partial \phi}{\partial n} = \phi(\frac{1}{r} - ik), \; on \; \Gamma_*. \tag{27}$$

Since p-enrichment is used, all the meshes are coarse and the mesh conforms exactly to the shape of the geometric model. The complex system defined by (15) in each example is solved by the use of an iterative solver based on pre-conditioned QMR technique [18].

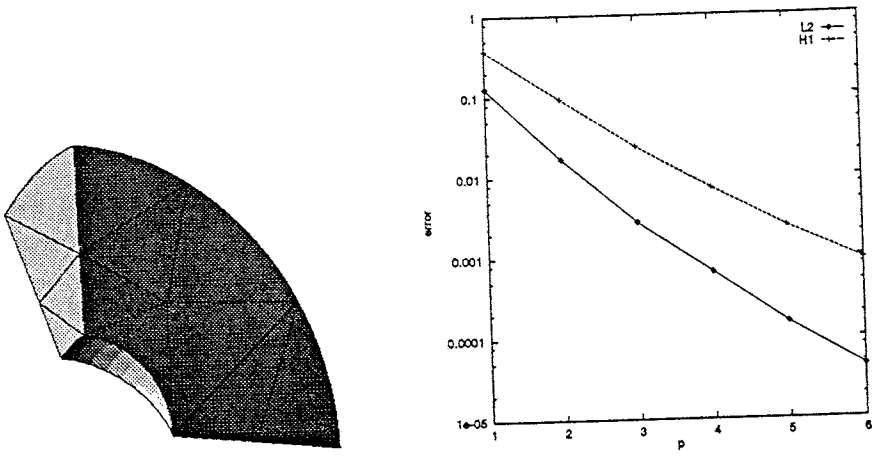

Figure 12: Mesh and convergence plot for radiation from a sphere.

The error in the finite element solution is measured in the normalized L_2 and the H_1-semi norm defined by

$$\|e\|_2 = \frac{\|(\phi - \phi^{(h,p)})\|_2}{\|\phi\|_2} = \frac{\sqrt{\int_{\Omega_f} (\phi - \phi^{(h,p)})\overline{(\phi - \phi^{(h,p)})} d\Omega}}{\sqrt{\int_{\Omega_f} \phi\bar{\phi} d\Omega}}, \tag{28}$$

$$|e|_1 = \frac{|(\phi - \phi^{(h,p)})|_1}{|\phi|_1} = \frac{\sqrt{\int_{\Omega_f} (\frac{\partial \phi}{\partial \mathbf{x}} - \frac{\partial \phi^{(h,p)}}{\partial \mathbf{x}})\overline{(\frac{\partial \phi}{\partial \mathbf{x}} - \frac{\partial \phi^{(h,p)}}{\partial \mathbf{x}})} d\Omega}}{\sqrt{\int_{\Omega_f} \frac{\partial \phi}{\partial \mathbf{x}} \overline{\frac{\partial \phi}{\partial \mathbf{x}}} d\Omega}}, \tag{29}$$

respectively, where the over-line indicates complex conjugation.

5.1 Radiation From Sphere

Γ_s is defined to be a sphere. Due to symmetry of the solution, one-half of a 10 degree slice of Ω_f is modeled consisting of 18 curvilinear tetrahedra. Figure 12 shows the mesh and the exponential rate of convergence of the normalized error in L_2 and H_1-semi norm. Figure 13 shows the iso-surfaces of the real component of the exact solution and that of the finite element solution for $p = 1, 3, 6$. The error with $p = 1$ in L_2 and H_1-semi norms are 13% and 38%, respectively; however, with $p = 6$ the corresponding error are dramatically reduced to 0.004% and 0.09%, respectively.

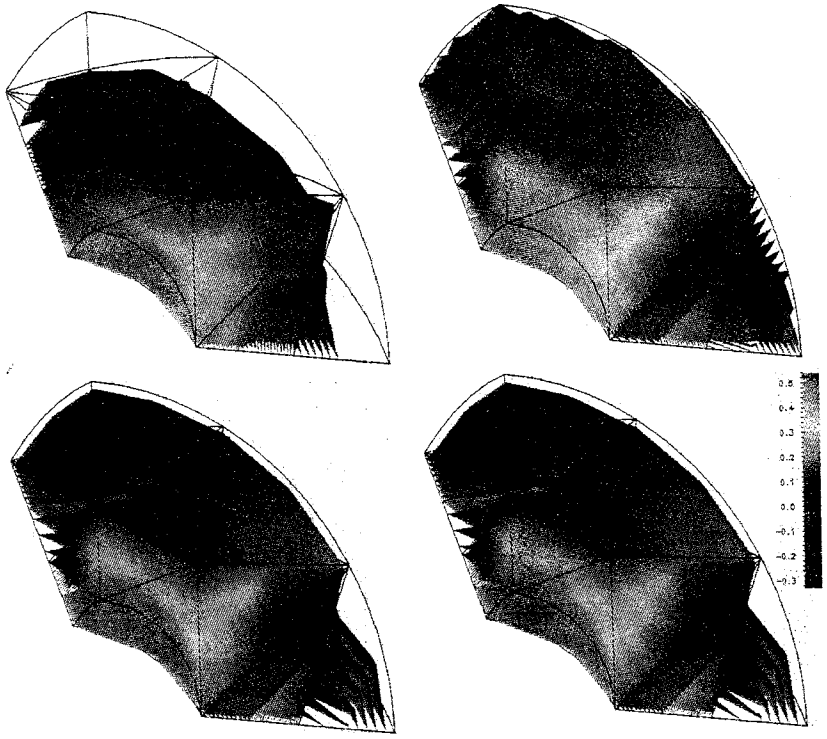

Figure 13: Iso-surfaces of real component of ϕ for sphere example: exact solution (top-left), $p = 1$ (top-right), $p = 3$ (bottom-left) and $p = 6$ (bottom-right).

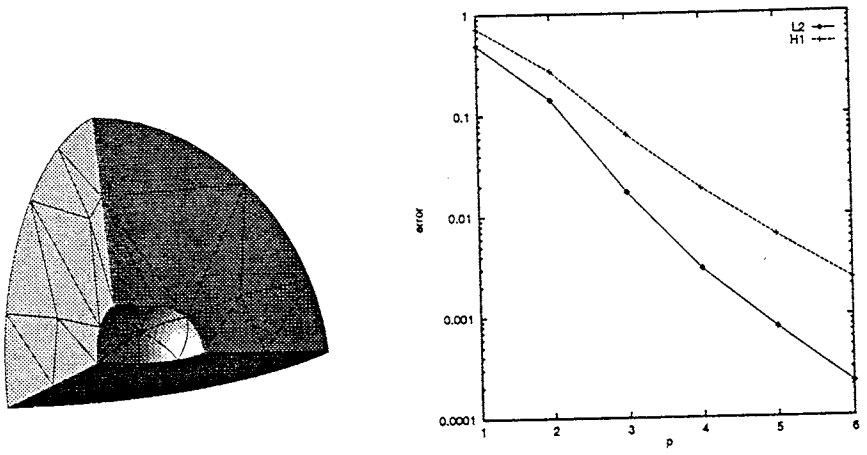

Figure 14: Mesh and convergence plot for radiation from a capped-cylinder.

5.2 Radiation From Capped Cylinder

Γ_s is defined by the skin of a cylinder with spherical end-caps. Due to symmetry of the solution, one-half of a 90 degree slice of Ω_f is modeled with 56 tetrahedra. Figure 14 shows the mesh and the convergence plot showing exponential rates. Figure 15 shows the iso-surfaces of the real component of the exact solution and that of the finite element solution for $p = 1, 3, 6$. The error with $p = 1$ in L_2 and H_1-semi norms are 49% and 73%, respectively; however, with $p = 6$ the corresponding error are dramatically reduced to 0.02% and 0.23%, respectively.

5.3 Radiation From Submarine

Γ_s is defined by the skin of a submarine-like body. Due to symmetry of the solution, one-half of of Ω_f is modeled as shown in Figure 16. The mesh consists of 2569 tetrahedral regions. Figure 17 shows the convergence of the finite element error along with the iso-surfaces of the real component of the exact solution and that of the finite element solution for $p = 1, 2, 3$. The errors with $p = 1$ in L_2 and H_1-semi norms are 67% and 76%, respectively, and those for $p = 3$ are 16% and 19%, respectively. Results for $p > 3$ could not be obtained because of the inability of the iterative solver to converge due to ill-conditioned systems that result from high-p methods [2].

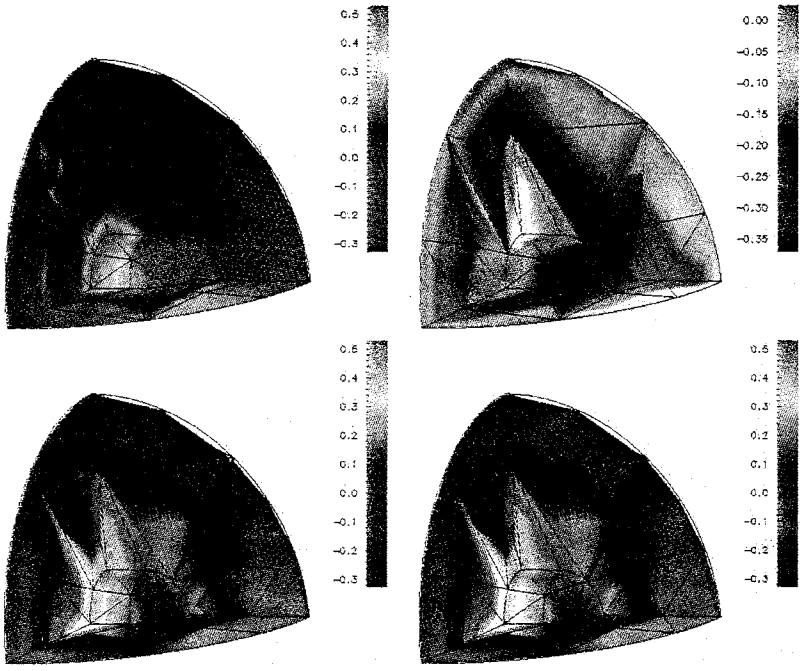

Figure 15: Iso-surfaces of real component of ϕ for capped-cylinder example: exact solution (top-left), $p = 1$ (top-right), $p = 3$ (bottom-left) and $p = 6$ (bottom-right).

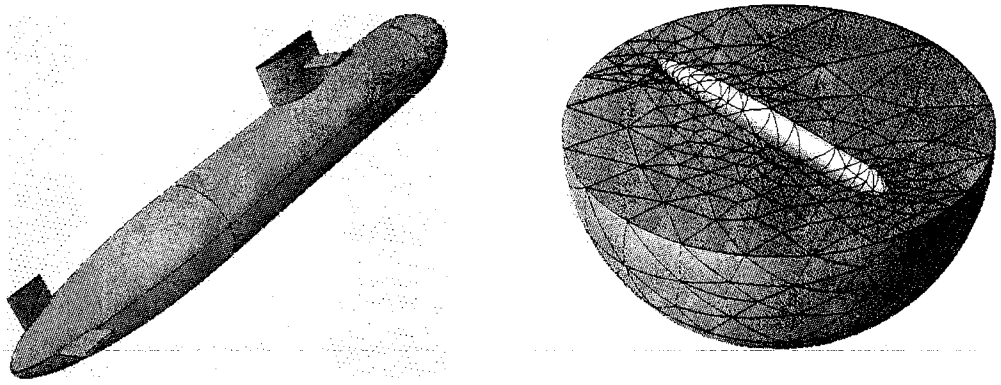

Figure 16: Model and mesh for radiation from submarine.

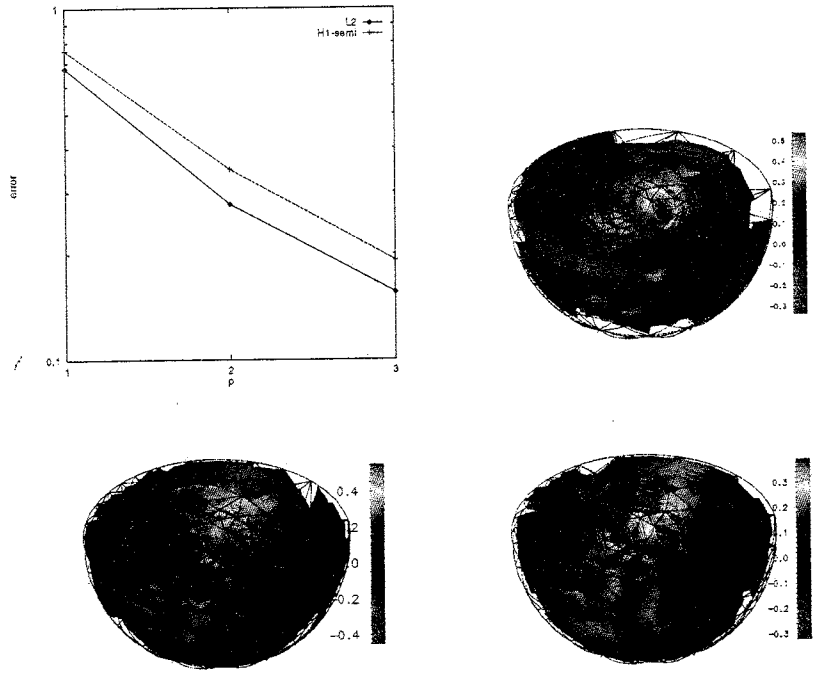

Figure 17: Submarine example: error convergence (top left) and iso-surfaces of real component of ϕ exact (top right), $p = 1$ (bottom left) and $p = 3$ (bottom right).

6 Closing Remarks

This paper has presented a technique the for accurate solution of the exterior Helmholtz equation in complex, curved three-dimensional domains. Based on the numerical examples presented, the following conclusion can be drawn: p-version Galerkin finite elements will provide excellent accuracy, even with coarse meshes, provided p is high and geometric mapping is accurate. However, stabilized methods are also a viable alternative to control dispersion. Numerical investigations into the computational cost of realizing a given level of solution accuracy with the use of stabilized h-methods and un-stabilized p-methods are needed determine the best discretization strategy. Stabilized p-version finite elements may turn out to be the ideal solution; however, GLS [17] type approach introduces additional complexities, for example, unlike linear elements, the second order derivatives are non-zero for $p > 1$ requiring second order derivatives of the shape functions and the geometric mapping functions.

The need for a robust, sparse, iterative solver that can handle poorly conditioned, indefinite, complex systems is born out by the numerical experiments.

7 Acknowledgments

Results presented in this paper were obtained using the computing resources of the Scientific Computation Research Center (SCOREC), Rensselaer Polytechnic Institute, Troy, NY 12180. The author is grateful to Prof. Mark. S. Shephard, Director, SCOREC, for access to its computers. The author also thanks Prof. Joseph E. Flaherty and Wesley Turner at the Department of Computer Science, Rensselaer Polytechnic Institute for many insightful discussions and the use of their iterative solver.

References

[1] N. N. Abboud and P. M. Pinsky. Finite element dispersion analysis for the three-dimensional second order scalar wave equation. *Int. J. Numer. Meth. Engng.*, 35:1183–1218, 1992.

[2] I. Babuska, M. Griebel, and J. Pitkaranta. The problem of selecting the shape functions for a p-type finite element. *Int. J. Numer. Meth. Engng.*, 28:1891–1908, 1989.

[3] I. Babuska and B. Q. Guo. Approximation properties of the h-p version of the finite element method. *Comp. Meth. Appl. Mech. Engng.*, 133:319–346, 1996.

[4] A. Bayliss, C. I. Goldstein, and E. Turkel. On accuracy conditions for the numerical computation of waves. *J. of Comp. Phy.*, 59:396–404, 1985.

[5] L. Demkowicz and J. T. Oden. Recent progress on application of *hp*-adaptive be/fe methods to elastic scattering. *J. of Acoust. Soc. Am.*, 96 (5):2798–2816, 1994.

[6] Saikat Dey. *Geometry-based three dimensional hp finite element modelling and computations.* PhD thesis, Civil Engineering, Rensselaer Polytechnic Institute, Scientific Computation Research Center, RPI, Troy, NY 12180-3590, January 1997.

[7] Saikat Dey, Mark S. Shephard, and Flaherty J. E. Geometry representation issues associated with p-version finite element computations. Technical Report SCOREC Report # 4-1997, Scientific Computation Research Center, Rensselaer Polytechnic Institute, Troy, NY 12180-3590, 1997. To appear: Special Issue of Computer Methods in Applied Mechanics and Engineering.

[8] I. Harari and T. J. R. Hughes. Finite element method for the helmholtz equation in an exterior domain: Model problems. *Comp. Meth. Appl. Mech. Engng.*, 87:59–96, 1991.

[9] T. J. R. Hughes. *The Finite Element Method: Linear Static and Dynamic Finite Element Analysis.* Prentice Hall, Englewood Cliffs, NJ, 1987.

[10] F. Ilhenburg and I. Babuska. Dispersion analysis and error estimation of galerkian finite element methods for the helmholtz equation. *Int. J. Numer. Meth. Engng.*, 38:3745–3774, 1995.

[11] J. T. Oden. Optimal h-p finite element methods. *Comp. Meth. Appl. Mech. Engng.*, 112:303–331, 1994.

[12] W. J. Schroeder and M. S. Shephard. On rigorous conditions for automatically generated finite element meshes. In J. Turner, J. Pegna, and M. Wozny, editors, *Product Modeling for Computer-Aided Design and Manufacturing*, pages 267–281. North Holland, 1991.

[13] M. S. Shephard, S. Dey, and J. E. Flaherty. A straight forward structure to construct shape functions for variable p-order meshes. *Comp. Meth. Appl. Mech. Engng.*, 147:209–233, 1997.

[14] M. S. Shephard and M. K. Georges. Reliability of automatic 3-D mesh generation. *Comp. Meth. Appl. Mech. Engng.*, 101:443–462, 1992.

[15] Joseph J. Shirron. *Solution of Exterior Helmholtz Problems Using Finite and Infinite Elements.* PhD thesis, Department of Applied Mathematics, University of Maryland, 1995.

[16] B. A. Szabo and I. Babuska. *Finite Element Analysis.* Wiley Interscience, New York, 1991.

[17] L. L. Thompson and P. M. Pinsky. A galerkin least squares finite element method for the two-dimensional helmholtz equation. *Int. J. Numer. Meth. Engng.*, 38:371–397, 1995.

[18] W. D. Turner, J. E. Flaherty, S. Dey, and M. S. Shephard. Multilevel preconditioned qmr methods for unstructured mesh computations. Technical report, Scientific Computation Research Center, Rensselaer Polytechnic Institute, Troy, NY 12180-3590, 1997. To appear: Special Issue of Computer Methods in Applied Mechanics and Engineering.

[19] O. C. Zienkiewicz and R. L. Taylor. *The Finite Element Method Volume 1 Basic Formulation and Linear Problems.* McGraw-Hill Book Company, London, 1989.